Journal of Biomechanics ▮ (▮▮▮▮) ▮▮▮–▮▮▮

Contents lists available at SciVerse ScienceDirect

Journal of Biomechanics

journal homepage: www.elsevier.com/locate/jbiomech
www.JBiomech.com

Tendon motion and strain patterns evaluated with two-dimensional ultrasound elastography

Laura A. Chernak [a,*], Darryl G. Thelen [a,b,c]

[a] Department of Biomedical Engineering, University of Wisconsin-Madison, USA
[b] Department of Mechanical Engineering, University of Wisconsin-Madison, USA
[c] Department of Orthopedics and Rehabilitation, University of Wisconsin-Madison, USA

ARTICLE INFO

Article history:
Accepted 7 August 2012

Keywords:
Tendon
Strain patterns
Ultrasound elastography

ABSTRACT

The purpose of this study was to evaluate the use of 2D ultrasound elastography to assess tendon tissue motion and strain under axial loading conditions. Four porcine flexor tendons were cyclically loaded to 4% peak strain using a servo hydraulic test system. An ultrasound transducer was positioned to image a longitudinal cross-section of the tendon during loading. Ultrasound radiofrequency (RF) data were collected at 63 frames per second simultaneously with applied force and crosshead displacement. A grid of nodes was manually positioned on an ultrasound image of the unloaded tendon. Small kernels (2×1 mm) centered at each node were then cross-correlated with search regions centered at corresponding nodal locations in the subsequent frame. Frame-to-frame nodal displacements were defined as the values that maximized the normalized cross-correlations. This process was repeated across all frames in the loading cycle, providing a measurement of the 2D trajectories of tissue motion throughout the loading cycle. The high resolution displacement measures along the RF beam direction were spatially differentiated to estimate the transverse (relative to tendon fibers) tissue strains. The nodal displacements obtained using this method were very repeatable, with average along-fiber trajectories that were highly correlated (average $r=0.99$) with the prescribed crosshead displacements. The elastography transverse strains were also repeatable and were consistent with average transverse strains estimated via changes in tendon width. The apparent Poisson's ratios (0.82–1.64) exceeded the incompressibility limit, but are comparable to values found for tendon in prior experimental and computational studies. The results demonstrate that 2D ultrasound elastography is a promising approach for noninvasively assessing localized tissue motion and strain patterns.

1. Introduction

Tendon injuries can be both chronic and debilitating. Tendinopathy, for example, is a painful overuse injury in which a localized region of tendinous tissue has degenerated (Maganaris et al., 2004; Sharma and Maffulli, 2005). Clinically, tendinopathies are challenging to resolve, which is due, in part, to the inconsistent response of patients to treatment protocols (Sharma and Maffulli, 2005). Thus, new imaging techniques are needed to elucidate the implications of localized tendon damage on function, and to quantitatively assess the effects of tissue repair or regeneration as a measure of treatment efficacy (Fleming and Beynnon, 2004). The development and use of new ultrasound analysis techniques can contribute to this goal by providing noninvasive assessments of tissue mechanics.

Ultrasound has become a ubiquitous tool in biomechanics for measuring tendon motion and strain in response to active muscle contractions. The most common method involves the collection and analysis of cine B-mode images of a tendon during loading and/or movement of the joint. The motion of an anatomical landmark(s) (e.g. the muscle–tendon junction) can be tracked across successive images to estimate average tendon strain (Maganaris, 2003; Maganaris and Paul, 1999; Maganaris and Paul, 2002; Peixinho et al., 2008). Prior studies using this method have provided fundamental insights into the relative stretch across the tendon, aponeurosis and muscle fascicles during in vivo loading conditions (Arampatzis et al., 2005; Arndt et al., 1998; Finni et al., 2003; Magnusson et al., 2003; Muramatsu et al., 2001). However, the anatomical feature tracking technique does not provide information on strain distributions, and therefore cannot assess the effect that tissue damage may have on localized tissue deformation.

* Correspondence to: Department of Biomedical Engineering, University of Wisconsin-Madison, 1513 University Ave, Rm 3046, Madison, WI 53706, USA. Tel.: +1 608 263 6692; fax: +1 608 265 2316.
E-mail address: lchernak@wisc.edu (L.A. Chernak).

0021-9290/$ - see front matter © 2012 Elsevier Ltd. All rights reserved.
http://dx.doi.org/10.1016/j.jbiomech.2012.08.001

Ultrasound elastography is an innovative technique for non-invasively assessing strain distributions within biological tissues. In standard elastography, ultrasound radiofrequency (RF) data are collected from a tissue in undeformed and deformed states (Varghese, 2009). The phase information inherent in the RF data can be used to accurately track the displacement of speckle patterns within the tissue along the ultrasound beam direction (Ophir et al., 1991). Spatial differentiation of displacement data is used to estimate the strain variations within the tissue (O'Donnell et al., 1994). Elastography has proven effective for detecting anomalies in soft tissues such as the breast, liver and thyroid, with deformation induced via simple manual compression of the tissue with the transducer (Inoue et al., 2010; Itoh et al., 2006; Lyshchik et al., 2005; Zhi et al., 2007). A few prior studies have assessed tendon deformation using this standard elastographic approach (De Zordo et al., 2009; Drakonaki et al., 2009). However, manual compression does not provide insights into how tendinous tissue will deform with active muscle loading, and thus likely does not represent the deformation patterns relevant to injury and rehabilitation.

A major challenge in elastographic imaging of normal tendon loading is that the primary direction of tissue motion is parallel to the surface of the skin, and therefore perpendicular to the ultrasound beam direction. Accurate 2D motion tracking is required to ensure that strains are computed for each tissue region as the tendon is translating within the image window. This can be difficult because the lateral resolution of ultrasound RF data is substantially lower than the along-beam resolution (Bohs and Trahey, 1991; Lopata et al., 2009; Ophir et al., 1999). A second challenge is that tendon can undergo large motion and deformation with muscle contraction, requiring that care must be taken to ensure that the tissue remains within the imaging plane and that accumulated motion is tracked over time. The purpose of this study, therefore, was to assess the capacity to use cine imaging and recent advances in 2D elastography (Chen et al., 2004; Ebbini, 2006; Huang and O'Donnell, 2010; Jiang and Hall, 2009; Lubinski et al., 1999) to evaluate tendon tissue motion and strain patterns under well-controlled axial loading conditions. We chose to use an *ex vivo* model such that applied force and displacement information could be directly compared to motion and strain data obtained using elastography. The results show a strong correlation between external and image-derived measures of tissue motion, suggesting that elastography shows promise as a tool for noninvasively assessing the relationship between tendon deformation and injury.

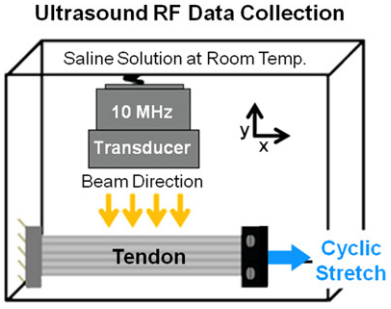

Fig. 1. Ultrasound RF data were collected from a longitudinal cross-section of the tendon during cyclic stretch.

2. Methods

We performed mechanical testing on four porcine flexor tendons using a servo hydraulic mechanical test system (Bionix858; MTS, Minneapolis, MN) with a custom bath (Fig. 1). The tendons were dissected from six-month old porcine specimens that were sacrificed for an unrelated study. The bony end of the tendon was secured in a metal block which was then loaded in a fixed grip. The insertion site was left intact at the distal end and embedded in lightweight filler (Evercoat, Cincinnati, OH). Tendons were kept hydrated with a phosphate buffered saline (PBS) solution during preparation. The specimens were wrapped in a PBS soaked towel and placed in a freezer in the time between dissection and testing. Tendons were fully thawed prior to mechanical testing. The insertion end of the tendon was then secured in a grip on the test machine crosshead that was attached to a 50 lb load cell (Eaton Corporation, Cleveland, OH), and testing was performed in a PBS solution filled bath. A 10 MHz, 38 mm wide linear array transducer (L14-5W/38, Ultrasonix Corporation, Richmond, BC, Canada) was secured in a holder and submerged in the bath such that RF data were provided from the midsection of the tendon. The transducer was aligned in the direction of the tendon fibers, and placed along the center axis of the tendon such that data were collected through the depth of the tendon from a longitudinal cross-section. Crosshead displacement and load cell data were simultaneously recorded with the ultrasound RF data.

Tendons were initially stretched to the point of onset of force development. The tendons were then pre-conditioned with cyclic stretch to 2% strain for ten cycles. Following a seven minute rest period, the tendons were sinusoidally stretched at 0.5 Hz to 4% peak strain for ten consecutive cycles. Ultrasonic RF data were collected over the final three cycles of motion. Three trials were performed for each specimen, with seven minutes of rest between cycles, such that data from a total of nine loading cycles were collected for each specimen. RF data were collected at a frame rate of 63 frames per second over a 38×30 mm image window. The image resolution was 128×1560, which provided a pixel size of 0.297×0.019 mm. It is notable that the beam direction resolution was substantially greater than the resolution in the direction perpendicular to the beam. Calipers were used to measure the two major diameters of the tendon cross-section prior to loading, and the cross-sectional area was computed by assuming that the tendon had an elliptical profile (Arruda et al., 2006).

A 2D ultrasound elastography algorithm was used to track tissue motion throughout each loading cycle (Fig. 2). To determine the tendon slack length, we measured the tendon length at the frame for which the applied force first

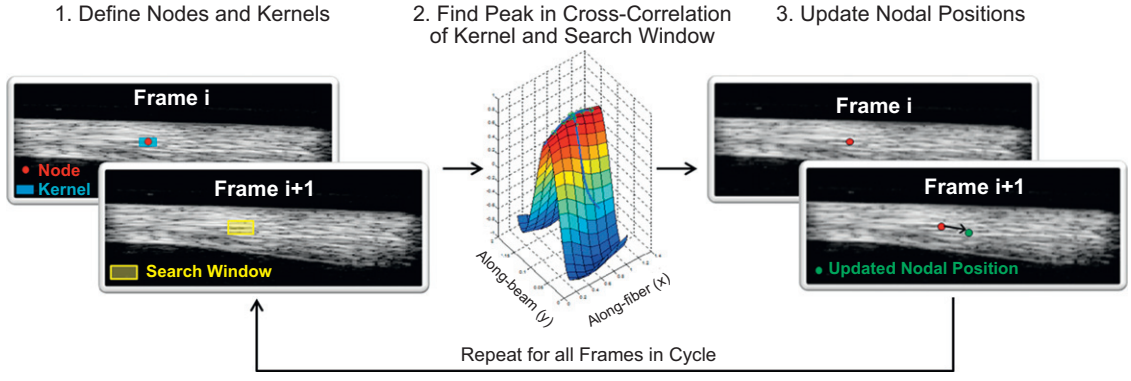

Fig. 2. Frame-to-frame tissue speckle tracking was performed by first defining nodes in Frame i and then centering kernels (2×1 mm) around the nodes (only one node is shown for illustrative purposes). Cross-correlations are then computed between the kernel and a search window (2.8×1.4 mm) in Frame i+1. The sharp peak in the cross-correlation function in the beam direction results from the phase information in RF data. The sub-pixel nodal displacements that maximize the correlation were found by fitting a 2D quartic spline to the correlation function near the nominal peak. The nodal positions are then updated (note: displacement vector is exaggerated for illustrative purposes) and the process is repeated for all frames within a loading cycle.

Please cite this article as: Chernak, L.A., Thelen, D.G., Tendon motion and strain patterns evaluated with two-dimensional ultrasound elastography. Journal of Biomechanics (2012), http://dx.doi.org/10.1016/j.jbiomech.2012.08.001

exceeded 5% of the peak tendon force. Tissue motion was then tracked until the frame at which the applied force dropped below 5% peak force. The RF images, force and displacement data for this time period were extracted. At each frame, cubic spline interpolation was used to upsample the RF data by a factor of 4 and 2 in the along-fiber (x) and along-beam (y) directions, respectively (Parker et al., 1983) (Table 1). Upsampling was performed to increase the spatial density of the correlation functions that were used to track tissue motion (Konofagou and Ophir, 1998). We then created a B-mode image of the unloaded tendon, and manually placed a grid of nodes along ~25 mm regions in the mid-tendon portion (Fig. 3a). The nodes were positioned every 1.0 and 0.5 mm along the x and y directions, and kernels (2×1 mm) were centered on the nodes. The nodes were positioned purposefully to ensure that the kernels used to estimate nodal displacements remained within the boundaries of the tendon throughout the loading cycle.

Table 1
Parameters used for 2D elastographic tracking of tissue motion.

	Along-fiber (x)	Along-beam (y)
Node spacing:	1.0 mm	0.5 mm
Kernel size:	2.0 mm	1.0 mm
Search window:	2.8 mm	1.4 mm
RF upsample rate:	4	2
Sub-pixel estimation:	2D Quartic Spline	
Spatial smoothing:	Median filter (3×3 nodes)	

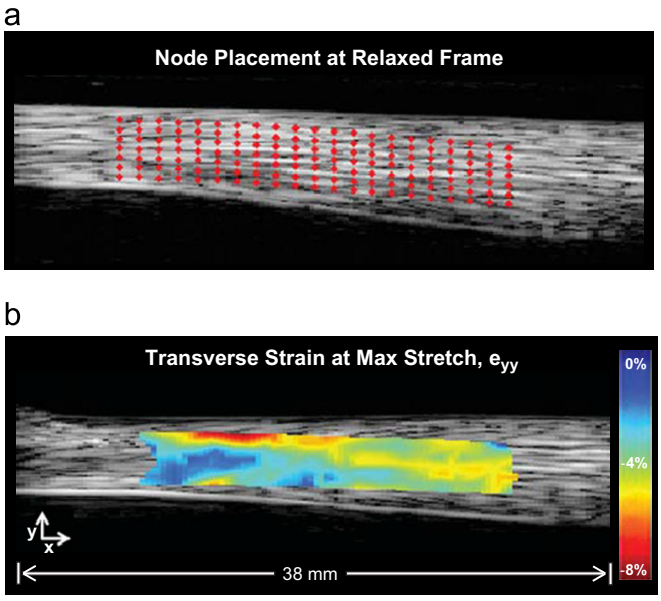

Fig. 3. (a) A Grid of nodes was placed along tendon fascicle direction in relaxed frame. (b) The Computed transverse tissue strains at most stretched position.

Frame-to-frame displacements were computed using a 2D normalized cross-correlation technique. Specifically, RF data within a kernel centered at the current node location were cross-correlated with RF data in a search region (2.8×1.4 mm) at the same location in the subsequent frame. The gross kernel displacements were first computed by finding the position that maximized the 2D correlation function. Sub-pixel displacements were then computed by fitting a 2D quartic spline to a 5×5 matrix of normalized correlations centered at the gross displacement value (Azar et al., 2010). A correlation threshold of $r=0.7$ was used to discriminate valid displacement information (Farron et al., 2009; Korstanje et al., 2009, 2010). Frame-to-frame displacements were median filtered (3×3 nodes) (Thitaikumar et al., 2008), and node positions were then updated by subsequently adding on the filtered displacements. These steps were repeated for all frames in a loading cycle to obtain the cumulative 2D displacement of each node. Motion tracking was also performed in the reverse direction by starting at the last frame and incrementing toward the first frame. A weighted average of the forward and backward nodal trajectories was then computed such that the final nodal trajectories were ensured to be cyclic in nature (Pelc et al., 1995).

Tissue strains in the y-direction (e_{yy}) were computed by numerically differentiating (3 point finite difference) the nodal y-displacement data relative to the initial nodal positions, and using a small strain approximation (Fig. 3b). The apparent Poisson's ratio was computed by taking the ratio of the negative transverse (e_{yy}) strain over the applied along-fiber (e_{xx}) strain from the final 50% of the loading phase (Smith et al., 1999). The change in transverse tendon width between the relaxed and stretched states was separately assessed via visual analysis of the B-mode images (Iwanuma et al., 2011). To do this, tendon width was measured at five locations along the tendon based on the center of the region of interest. The average transverse strain of the entire ROI was then computed based on the change in width at the five locations normalized to the unloaded tendon width. Analysis using both strain measurement techniques was repeated three times for each loading cycle to evaluate repeatability.

3. Results

The average elastographic nodal displacements along the tendon fascicle direction (x) agreed well with the prescribed crosshead displacements. Force–displacement curves derived from both measures demonstrated similar nonlinear strain-stiffening behavior (Fig. 4a). The along-fiber and crosshead displacements were highly linearly correlated, with average r^2 values greater than 0.98 (Fig. 4b). The ratio of along-fiber to crosshead displacement differed between specimens, but was extremely repeatable within the nine cycles for each specimen.

The average transverse strains at the most stretched frame varied between specimens, ranging from −2.5 to −8.5%. Average transverse strain magnitudes were comparable to measures of tendon width change, but exhibited substantially less variability across loading cycles (Fig. 5).

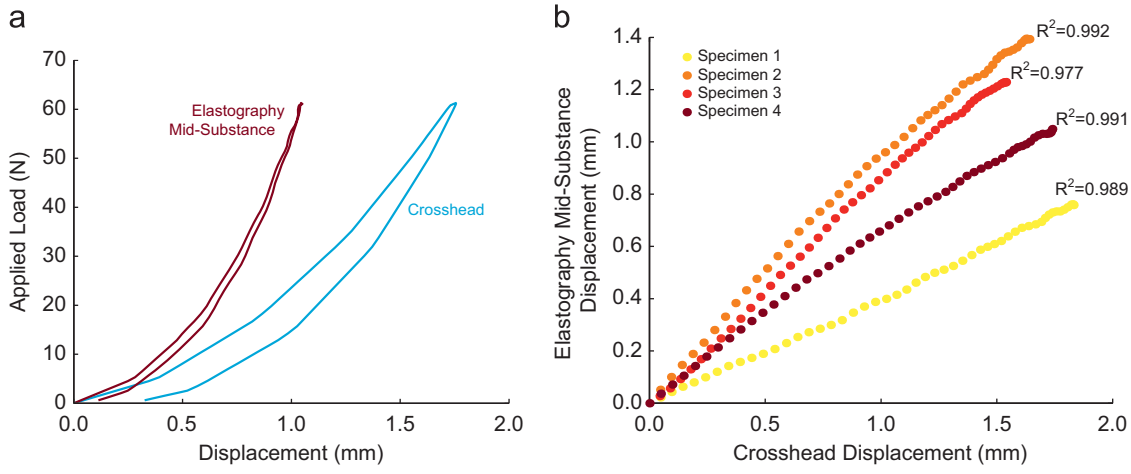

Fig. 4. (a) Displacement of the mid-substance tendon measured with elastography exhibited similar strain-stiffening behavior as the applied crosshead displacement. (b) Crosshead and elastography displacement data were highly correlated over the entire loading range.

Please cite this article as: Chernak, L.A., Thelen, D.G., Tendon motion and strain patterns evaluated with two-dimensional ultrasound elastography. Journal of Biomechanics (2012), http://dx.doi.org/10.1016/j.jbiomech.2012.08.001

At low strains, the average transverse strain magnitude within the ROI increased at a faster rate than the applied strain (Fig. 6a). The apparent Poisson's ratios computed using strains from the last half of the loading cycle ranged from 0.8 to 1.64 (Fig. 6b). Within a specimen, the coefficient of variation for the apparent Poisson's ratio ranged from 6–22% across the four specimens.

4. Discussion

This study was undertaken to evaluate the use of 2D elastography to assess tendon tissue motion and deformation with axial loading. We found that along-fiber displacement curves obtained via elastography correlated highly with the applied crosshead displacement, which is expected if the deformation pattern along the tendon axis is relatively invariant with loading. The elastographic transverse strain magnitudes differed between specimens, but all specimens exhibited a monotonic increase with the applied grip-to-grip strains (Fig. 6a). The apparent Poisson's ratio estimates exceeded 0.5 for all the tendon specimens, a phenomenon that has been previously been observed using other techniques (Cheng and Screen, 2007; Lynch et al., 2003; Vergari et al., 2011). All elastographic measures of displacement and strain were relatively consistent between repeat loading cycles of a specimen. Hence, we believe that RF elastography is a promising new approach for noninvasively measuring tissue motion and deformation under axial loading conditions.

Ultrasound is often used in biomechanics to measure average in vivo tendon motion and stretch with loading. This is commonly accomplished by collecting ultrasound B-mode images during a musculotendon contraction, and then retrospectively tracking the motion of an anatomical landmark at one end of the tendon (e.g. a muscle tendon junction) in the images. The motion at the other end of the tendon is then either estimated (Maganaris, 2003; Maganaris and Paul, 1999, 2002; Peixinho et al., 2008) or is tracked using a second transducer (Arndt et al., 2006). The difference in displacements between the two ends of the tendon provides an estimate of average tendon stretch (Arndt et al., 2006; Kongsgaard et al., 2011; Maganaris, 2003; Maganaris and Paul, 1999, 2002; Peixinho et al., 2008). The complex temporal relationship between average tendon and muscle fascicle stretch has been elucidated using such techniques (Fukunaga et al., 2002). However, this anatomical feature tracking approach can only provide an estimate of average strain and thus cannot distinguish strain variations within the tissue that are considered relevant to localized tendon injuries (Maganaris et al., 2004; Sharma and Maffulli, 2005).

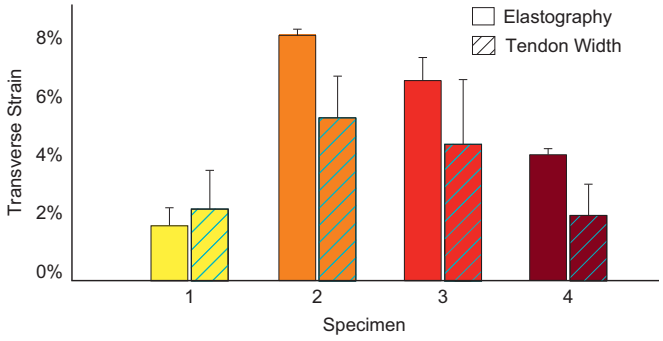

Fig. 5. Peak transverse strain magnitudes computed via elastography and ascertained via visual analysis of B-mode images. Strains were calculated three times for each of the nine repeat loading cycles (+1 s.d. shown). The two strain measures show similar results with more consistency for strains computed with elastography.

Ultrasound elastography is an automated imaging based tool for characterizing spatial variations in tissue motion and strain. Fundamental to elastography is the use of RF data, which allows one to use small shifts in the phase of the reflected sound wave to ascertain the motion of speckles along the ultrasound beam direction (Varghese, 2009). In fact, a recent theoretical study showed that elastographic motion estimates obtained using RF data resulted in more accurate displacement measures than what can be obtained using B-mode images (Lopata et al., 2009). To assess this effect in our data, we computed the full width half maximum (FWHM) of the autocorrelation of the region of interest within the tendon for all images. Correlations obtained with RF data exhibited a sharper peak than those obtained from the B-mode data, with the average FWHM found to be 0.12 mm and 0.45 mm, respectively. FWHM was substantially larger (2.7 mm) in the direction perpendicular to the ultrasound beam, which is related to the difference in spacing between the RF lines (0.296 mm) and between the samples along the beam direction (0.019 mm). Although lateral motion tracking is less precise, the importance of 2D motion tracking has increasingly been recognized, and previous studies have used a variety of techniques to attain 2D elastographic tracking including plane strain assumptions (Lubinski et al., 1996; Righetti et al., 2003), synthetic phase (Chen et al., 2004; Huang and O'Donnell, 2010) and 2D cross-correlation techniques (Ebbini, 2006; Kaluzynski et al., 2001; Trahey et al., 1987). We chose to use the 2D normalized cross-correlation function with quartic spline interpolation, because it has been shown to result in substantially lower bias errors than using lower-order polynomial or cosine fits to the correlation function (Azar et al., 2010). An inherent advantage of the elastographic technique is that it is capable of estimating strain

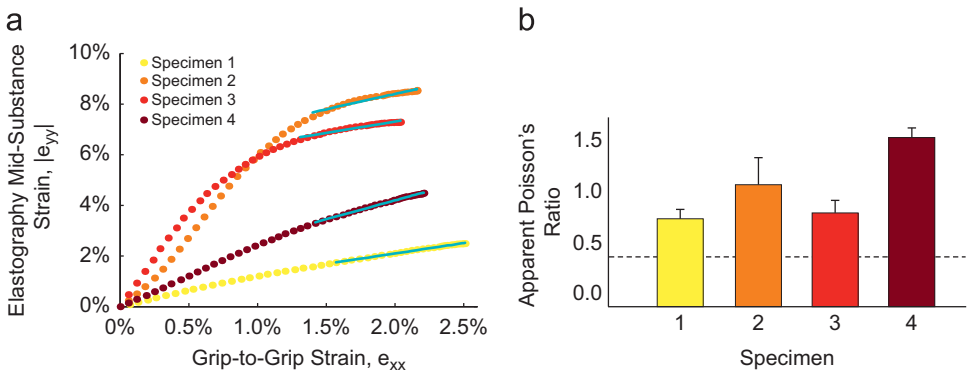

Fig. 6. (a) Average transverse strains ($|e_{yy}|$) increase faster than grip-to-grip strain (e_{xx}) at low loads, before settling in a more linear relationship. (b) Each specimen exhibited a Poisson's ratio that exceeded the incompressibility limit for isotropic materials (0.5).

Please cite this article as: Chernak, L.A., Thelen, D.G., Tendon motion and strain patterns evaluated with two-dimensional ultrasound elastography. Journal of Biomechanics (2012), http://dx.doi.org/10.1016/j.jbiomech.2012.08.001

variations within the image window, which obviates the need for multiple transducers or making assumptions about motion outside the image window.

The apparent Poisson's ratios found in this study ranged from 0.82 to 1.64. These values are comparable to literature estimates of Poisson's ratio ranging from 0.55 to 2.98 for tendon (Cheng and Screen, 2007; Lynch et al., 2003; Vergari et al., 2011) found using other methods, and is consistent with the findings for other transversely isotropic materials (Lempriere, 1968). An apparent Poisson's ratio greater than 0.5 exceeds the incompressibility limit for isotropic materials, and reflects volume loss with stretch (Lanir et al., 1988). Physiologically, it is possible that this volume loss could arise from the exudation of fluid during stretch. A recent micromechanical tendon model investigated this issue and found that the apparent Poisson's ratio can greatly exceed the incompressibility limit, and its value is heavily dependent on the helical pitch and crimp angles of the fibers (Reese et al., 2010). In addition, the helical organization of tendon fibrils result in a load-dependent Poisson's ratio, with the highest values for strains below ~1.5% (Reese et al., 2010). Similarly, we found the transverse strains increased faster than the applied strains at low loads, before settling to a more constant ratio at higher loads (Fig. 6a). The strong dependence of Poisson's ratio on specific structural features may explain the variation between specimens that have been noted in other studies (Cheng and Screen, 2007; Lynch et al., 2003; Vergari et al., 2011), as well as in the current study. The elastographic transverse strain patterns were non-uniform across the tendon, but highly consistent between repeat loading cycles and generally consistent with tendon width measures as ascertained from the B-mode images (Fig. 5). Non-uniform strain patterns have also been observed when using optical markers to track surface strains (Cheng and Screen, 2007), and could reflect variations in morphological structure as well as experimental factors such as specimen mounting and gripping.

As with other ultrasound approaches, we were only able to track tissue motion that occurred within the image window. We sought to minimize potential out-of-plane motion by fixing the transducer in space to continuously capture images from a cross-section of the tendon along the direction of the tendon fibers. We also collected RF data at a frame rate of 63 frames per second such that frame-to-frame motion was relatively low. The small frame-to-frame displacements increased the potential to keep scatterers in view, which decreases the effect of out-of-plane motion and therefore enhances the ability to accurately track motion (Ophir et al., 1999). The normalized cross-correlations of kernels were quite high (average $r=0.99$), reflecting a small amount of decorrelation was occurring between successive frames. A lower frame rate (33.5 Hz) was considered by skipping a frame in the tracking process. This reduced the correlations slightly (average $r=0.98$), but did not appreciably affect the cumulative tracking results. We note that when using incremental elastographic techniques it becomes more challenging to keep the region of interest within the image window if the tissue undergoes large rigid body motion or extremely large deformation. This is more likely to occur if the technique is used to track aponeurosis and muscle tissue motion. Therefore, in future studies, it will be important to assess the effects of out-of-plane motion on elastographic strain measures along and transverse to the sound beam, an issue which may be well suited for investigation with an ultrasound phantom.

In conclusion, we have demonstrated the potential to use 2D ultrasound elastography to quantitatively assess tendon tissue motion and strains with loading that are consistent with experimental measures and previous studies. The approach provides regional strain information that could prove relevant for quantitatively assessing tissue strain patterns following injury and clinical treatment.

Conflict of interest statement

None.

Acknowledgments

NIH AR056201, American Society of Biomechanics Grant-in-Aid Program, Ryan DeWall, Sarah Duenwald Kuehl, Kayt Frisch, Ray Vanderby, Tomy Varghese, Dan Volk.

References

Arampatzis, A., Stafilidis, S., DeMonte, G., Karamanidis, K., Morey-Klapsing, G., Bruggenmann, G.P., 2005. Strain and elongation of the human gastrocnemius tendon and aponeurosis during maximal plantarflexion effort. Journal of Biomechanics 38, 833–841.

Arndt, A., Tomatis, L., Ryberg, A., Kleman, D., Peolsson, M., Thorstensson, A., 2006. In vivo sonometry measurement of strain in the human achilles tendon. Journal of Biomechanics 39, S495.

Arndt, A.N., Komi, P.V., Bruggemann, G.P., Lukkariniemi, J., 1998. Individual muscle contributions to the in vivo achilles tendon force. Clinical Biomechanics 13, 532–541.

Arruda, E.M., Calve, S., Dennis, R.G., Mundy, K., Baar, K., 2006. Regional variation of tibialis anterior tendon mechanics is lost following denervation. Journal of Applied Physiology 101, 1113–1117.

Azar, R.Z., Goksel, O., Salcudean, S.E., 2010. Sub-sample displacement estimation from digitized ultrasound rf signals using multi-dimensional polynomial fitting of the cross-correlation function. IEEE Transactions on Ultrasonics, Ferroelectrics, and Frequency Control 57, 2403–2420.

Bohs, L.N., Trahey, G.E., 1991. A novel method for angle independent ultrasonic-imaging of blood-flow and tissue motion. IEEE Transactions on Biomedical Engineering 38, 280–286.

Chen, X.C., Zohdy, M.J., Emelianov, S.Y., O'Donnell, M., 2004. Lateral speckle tracking using synthetic lateral phase. IEEE Transactions on Ultrasonics, Ferroelectrics, and Frequency Control 51, 540–550.

Cheng, V.W.T., Screen, H.R.C., 2007. The micro-structural strain response of tendon. Journal of Materials Science 42, 8957–8965.

De Zordo, T., Lill, S.R., Fink, C., Feuchtner, G.M., Jaschke, W., Bellmann-Weiler, R., Klauser, A.S., 2009. Real-time sonoelastography of lateral epicondylitis: comparison of findings between patients and healthy volunteers. American Journal of Roentgenology 193, 180–185.

Drakonaki, E., Allen, G., Wilson, D., 2009. Real-time ultrasound elastography of the normal achilles tendon: reproducibility and pattern description. Clinical Radiology 64, 1196–1202.

Ebbini, E.S., 2006. Phase-coupled two-dimensional speckle tracking algorithm. IEEE Transactions on Ultrasonics, Ferroelectrics, and Frequency Control 53, 972–990.

Farron, J., Varghese, T., Thelen, D.G., 2009. Measurement of tendon strain during muscle twitch contractions using ultrasound elastography. IEEE Transactions on Ultrasonics, Ferroelectrics, and Frequency Control 56, 27–35.

Finni, T., Hodgson, J.A., Lai, A.M., Edgerton, V.R., Sinha, S., 2003. Nonuniform strain of human soleus aponeurosis-tendon complex during submaximal voluntary contractions in vivo. Journal of Applied Physiology 95, 829–837.

Fleming, B.C., Beynnon, B.D., 2004. In vivo measurement of ligament/tendon strains and forces: a review. Annals of Biomedical Engineering 32, 318–328.

Fukunaga, T., Kawakami, Y., Kubo, K., Kanehisa, H., 2002. Muscle and tendon interaction during human movements. Exercise and Sport Sciences Reviews 30, 106–110.

Huang, L., O'Donnell, M., 2010. A synthetic lateral phase (SLP) displacement estimator using complex FIR filters. IEEE Ultrasonics Symposium, 1996–1999.

Inoue, Y., Takahashi, M., Arita, J., Aoki, T., Hasegawa, K., Beck, Y., Makuuchi, M., Kokudo, N., 2010. Intra-operative freehand real-time elastography for small focal liver lesions: "visual palpation" for non-palpable tumors. Surgery 148, 1000–1011.

Itoh, A., Ueno, E., Tohno, E., Kamma, H., Takahashi, H., Shiina, T., Yamakawa, M., Matsumura, T., 2006. Breast disease: clinical application of us elastography for diagnosis. Radiology 239, 341–350.

Iwanuma, S., Akagi, R., Kurihara, T., Ikegawa, S., Kanehisa, H., Fukunaga, T., Kawakami, Y., 2011. Longitudinal and transverse deformation of human achilles tendon induced by isometric plantar flexion at different intensities. Journal of Applied Physiology 110, 1615–1621.

Jiang, J., Hall, T.J., 2009. A generalized speckle tracking algorithm for ultrasonic strain imaging using dynamic programming. Ultrasound in Medicine & Biology 35, 1863–1879.

Kaluzynski, K., Chen, X.C., Emelianov, S.Y., Skovoroda, A.R., O'Donnell, M., 2001. Strain rate imaging using two-dimensional speckle tracking. IEEE Transactions on Ultrasonics, Ferroelectrics, and Frequency Control 48, 1111–1123.

Kongsgaard, M., Nielsen, C.H., Hegnsvad, S., Aagaard, P., Magnusson, S.P., 2011. Mechanical properties of the human achilles tendon, in vivo. Clinical Biomechanics 26, 772–777.

Please cite this article as: Chernak, L.A., Thelen, D.G., Tendon motion and strain patterns evaluated with two-dimensional ultrasound elastography. Journal of Biomechanics (2012), http://dx.doi.org/10.1016/j.jbiomech.2012.08.001

Konofagou, E., Ophir, J., 1998. A new elastographic method for estimation and imaging of lateral displacements, lateral strains, corrected axial strains and Poisson's ratios in tissues. Ultrasound in Medicine & Biology 24, 1183–1199.

Korstanje, J., Selles, R., Henk, S., Hovius, S., Bosch, J., 2009. Dedicated ultrasound speckle tracking to study tendon displacement. In: Conference Proceedings of SPIE Medical Imaging 2009: Ultrasonic Imaging and Signal Processing. Lake Buena Vista, FL, USA.

Korstanje, J.W., Selles, R.W., Stam, H.J., Hovius, S.E., Bosch, J.G., 2010. Development and validation of ultrasound speckle tracking to quantify tendon displacement. Journal of Biomechanics 43, 1373–1379.

Lanir, Y., Salant, E.L., Foux, A., 1988. Physico-chemical and microstructural changes in collagen fiber bundles following stretch in-vitro. Biorheology 25, 591–603.

Lempriere, B.M., 1968. Poissons ratio in orthotropic materials. American Institute of Aeronautics and Astronautics Journal 6, 2226–2227.

Lopata, R., Nillesen, M., Hansen, H., Gerrits, I., Thijssen, J., de Korte, C., 2009. Performance evaluation of methods for two-dimensional displacement and strain estimation using ultrasound radio frequency data. Ultrasound in Medicine & Biology 35, 796–812.

Lubinski, M.A., Emelianov, S.Y., O'Donnell, M., 1999. Speckle tracking methods for ultrasonic elasticity imaging using short-time correlation. IEEE Transactions on Ultrasonics, Ferroelectrics, and Frequency Control 46, 82–96.

Lubinski, M.A., Emelianov, S.Y., Raghavan, K.R., Yagle, A.E., Skovoroda, A.R., ODonnell, M., 1996. Lateral displacement estimation using tissue incompressibility. IEEE Transactions on Ultrasonics, Ferroelectrics, and Frequency Control 43, 247–256.

Lynch, H.A., Johannessen, W., Wu, J.P., Jawa, A., Elliott, D.M., 2003. Effect of fiber orientation and strain rate on the nonlinear uniaxial tensile material properties of tendon. Journal of Biomechanical Engineering 125, 726–731.

Lyshchik, A., Higashi, T., Asato, R., Tanaka, S., Ito, J., Mai, J.J., Pellot-Barakat, C., Insana, M.F., Brill, A.B., Saga, T., Hiraoka, M., Togashi, K., 2005. Thyroid gland tumor diagnosis at us elastography. Radiology 237, 202–211.

Maganaris, C.N., 2003. Tendon conditioning: artefact or property? Proceedings of the Royal Society—Biological Sciences 270 (Suppl. 1), S39–S42.

Maganaris, C.N., Narici, M.V., Almekinders, L.C., Maffulli, N., 2004. Biomechanics and pathophysiology of overuse tendon injuries: ideas on insertional tendinopathy. Sports Medicine 34, 1005–1017.

Maganaris, C.N., Paul, J.P., 1999. In vivo human tendon mechanical properties. Journal of Physiology 521 (Pt 1), 307–313.

Maganaris, C.N., Paul, J.P., 2002. Tensile properties of the in vivo human gastrocnemius tendon. Journal of Biomechanics 35, 1639–1646.

Magnusson, S.P., Hansen, P., Aagaard, P., Brond, J., Dyhre-Poulsen, P., Bojsen-Moller, J., Kjaer, M., 2003. Differential strain patterns of the human gastrocnemius aponeurosis and free tendon, in vivo. Acta Physiologica Scandinavica 177, 185–195.

Muramatsu, T., Muraoka, T., Takeshita, D., Kawakami, Y., Hirano, Y., Fukunaga, T., 2001. Mechanical properties of tendon and aponeurosis of human gastrocnemius muscle in vivo. Journal of Applied Physiology 90, 1671–1678.

O'Donnell, M., Skovoroda, A.R., Shapo, B.M., Emelianov, S.Y., 1994. Internal displacement and strain imaging using ultrasonic speckle tracking. IEEE Transactions on Ultrasonics, Ferroelectrics, and Frequency Control 41, 314–325.

Ophir, J., Alam, S.K., Garra, B., Kallel, F., Konofagou, E., Krouskop, T., Varghese, T., 1999. Elastography: ultrasonic estimation and imaging of the elastic properties of tissues. Proceedings of the Institution of Mechanical Engineers. Part H: Journal of Engineering in Medicine 213, 203–233.

Ophir, J., Céspedes, I., Ponnekanti, H., Yazdi, Y., Li, X., 1991. Elastography: a quantitative method for imaging the elasticity of biological tissues. Ultrasonic Imaging 13, 111–134.

Parker, J., Kenyon, R.V., Troxel, D.E., 1983. Comparison of interpolating methods for image resampling. IEEE Transactions on Medical Imaging 2, 31–39.

Peixinho, C.C., Alves, D.S., Lacerda, R.G., Vieira, T.M.M., Oliveira, L.F., 2008. Strain and slackness of achilles tendon during passive joint mobilization via imaging ultrasonography. Revista Brasileira De Fisioterapia 12, 366–372.

Pelc, N.J., Drangova, M., Pelc, L.R., Zhu, Y., Noll, D.C., Bowman, B.S., Herfkens, R.J., 1995. Tracking of cyclic motion with phase-contrast cine mr velocity data. Journal of Magnetic Resonance Imaging: JMRI 5, 339–345.

Reese, S.P., Maas, S.A., Weiss, J.A., 2010. Micromechanical models of helical superstructures in ligament and tendon fibers predict large poisson's ratios. Journal of Biomechanics 43, 1394–1400.

Righetti, R., Srinivasan, S., Ophir, J., 2003. Lateral resolution in elastography. Ultrasound in Medicine & Biology 29, 695–704.

Sharma, P., Maffulli, N., 2005. Tendon injury and tendinopathy: healing and repair. Journal of Bone and Joint Surgery 87, 187–202.

Smith, C.W., Wootton, R.J., Evans, K.E., 1999. Interpretation of experimental data for poisson's ratio of highly nonlinear materials. Experimental Mechanics 39, 356–362.

Thitaikumar, A., Mobbs, L.M., Kraemer-Chant, C.M., Garra, B.S., Ophir, J., 2008. Breast tumor classification using axial shear strain elastography: a feasibility study. Physics in Medicine and Biology 53, 4809–4823.

Trahey, G.E., Allison, J.W., Vonramm, O.T., 1987. Angle independent ultrasonic-detection of blood-flow. IEEE Transactions on Biomedical Engineering 34, 965–967.

Varghese, T., 2009. Quasi-static ultrasound elastography. Ultrasound Clinics 4, 323–338.

Vergari, C., Pourcelot, P., Holden, L., Ravary-Plumioen, B., Gerard, G., Laugier, P., Mitton, D., Crevier-Denoix, N., 2011. True stress and Poisson's ratio of tendons during loading. Journal of Biomechanics 44, 719–724.

Zhi, H., Ou, B., Luo, B.M., Feng, X., Wen, Y.L., Yang, H.Y., 2007. Comparison of ultrasound elastography, mammography, and sonography in the diagnosis of solid breast lesions. Journal of Ultrasound in Medicine: Official Journal of the American Institute of Ultrasound in Medicine 26, 807–815.

Please cite this article as: Chernak, L.A., Thelen, D.G., Tendon motion and strain patterns evaluated with two-dimensional ultrasound elastography. Journal of Biomechanics (2012), http://dx.doi.org/10.1016/j.jbiomech.2012.08.001